LBL-25657

Lawrence Berkeley Laboratory
UNIVERSITY OF CALIFORNIA

EARTH SCIENCES DIVISION

Invited paper to be presented at the International Conference on Fluid Flow in Fractured Rocks, Atlanta, GA, May 16–18, 1988

Tracer Transport in Fractured Rocks

C.F. Tsang, Y.W. Tsang, and F.V. Hale

July 1988

Prepared for the U.S. Department of Energy under Contract Number DE-AC03-76SF00098.

DISCLAIMER

LBL--25657

DE89 001258

Invited Paper, International Conference
on Fluid Flow in Fractured Rocks,
Atlanta, Georgia, May 16-18, 1988

Tracer Transport in Fractured Rocks

C. F. Tsang, Y. W. Tsang and F. V. Hale

Earth Sciences Division
Lawrence Berkeley Laboratory
University of California
Berkeley, California 94720

Abstract

Recent interest in the safety of toxic waste underground disposal and nuclear waste geologic repositories has motivated many studies of tracer transport in fractured media. Fractures occur in most geologic formations and introduce a high degree of heterogeneity. Within each fracture, the aperture is not constant in value but strongly varying. Thus for such media, tracer tends to flow through preferred flowpaths or channels within the fractures. Along each of these channels, the aperture is also strongly varying.

A detailed analysis is carried out on a 2D single fracture with variable apertures and the flow through channels is demonstrated. The channels defined this way are not rigidly set pathways for tracer transport, but are the preferred flow paths in the sense of stream-tubes in the potential theory. It is shown that such variable-aperture channels can be characterized by an aperture probability distribution function, and not by the exact deterministic geometric locations. We also demonstrate that the 2D tracer transport in a fracture can be calculated by a model of a system of 1D channels characterized by this distribution function only. Due to the channeling character of tracer transport in fractured rock, random point measurements of tracer breakthrough curves may give results with a wide spread in value due to statistical fluctuations. The present paper suggests that such a wide spread can probably be greatly reduced by making line/areal (or multiple) measurements covering a few spatial correlation lengths.

Introduction

Recent interest in the evaluation of contaminant transport in bedrock aquifers and in the performance assessment of a geologic nuclear waste repository has motivated many studies of tracer transport in fractured rocks. Some of these studies have assumed that fractures can be represented by disks with constant apertures. This is what is called the parallel-plate model. The experiments of Abelin et al. (1982) in the Stripa mines in Sweden first brought out the inadequacy of the parallel plate idealization of a fracture. They showed that the mean parallel-plate aperture deduced from flow permeability data and that inferred from tracer transport time data differ by as much as one order of magnitude. The variable-aperture nature of single fractures can lead to the above observations (see e.g. Tsang, 1984).

The variable apertures in a fracture give rise to a very heterogeneous system. Tracer particles flowing through such a system tend to follow paths of least resistance. Evidence that flow in fractures tends to coalesce in preferred paths has been found in the field (e.g. Neretnieks, 1985; and Bourke, 1987). Motivated by these data, Tsang and Tsang (1987) proposed the variable-aperture channel model for transport through fractured media. The properties of the channel model were further developed by Tsang et al. (1988) and the channeling characteristics of flow through a two-dimensional single fracture were analyzed in detail by Moreno et al. (1988).

The purpose of the present paper is to show how a detailed flow calculation in a two-dimensional variable-aperture single fracture gives rise to flow channeling. Because of the channeling effect, point measurements of tracer transport in the highly heterogeneous single fracture may give results with large fluctuations in value. The use of line, areal or multi-point measurements provides a way to reduce the spread of the fluctuations and to correlate the mean of the measured values to the fracture aperture parameters. Finally, we show how the tracer transport through a 2D single

fracture with strongly variable apertures can be simulated with 1D variable-aperture channels, which are characterized by an aperture probability distribution function with two parameters.

Channeling in 2D single fractures with strongly varying apertures

In this section we shall demonstrate the channeling characteristics of flow in a 2D single fracture with strongly varying apertures. We use an aperture density distribution for the aperture values over the single fracture. Measurements of aperture values were made by Gentier (1986) and Gale (this volume, 1988) in laboratory core samples. Based on their results, we assume that these aperture values obey a lognormal distribution, which is characterized by two parameters, the (arithmetic) mean aperture value, $\bar{b}$, and standard deviation (in log b), σ. The arithmetic mean is taken here because it is a well-defined quantity related to tracer transport. Figure 1 shows three distributions with the same value of $\bar{b}$ and different values of σ on a linear scale. It is of interest to note that as σ increases, the peak location of the distribution decreases and the half-widths of the distribution in b also decreases. If the distribution were plotted on a log scale, the half-width in log b would indeed increase with σ (Tsang et al. 1988).

Given the aperture distribution, the single fracture with variable aperture is constructed by means of standard geostatistical methods in a procedure described in Moreno et al. (1988). A number of realizations were generated. Here, we have introduced a third parameter, the spatial correlation length λ which is a measure of the distance over which the apertures are correlated. In this study we have assumed the system to be isotropic. Figure 2 shows one such realization, based on a lognormal distribution with $\bar{b} = 82$ μm, $\sigma = 0.43$ and $\lambda = 0.1L$, where L is the dimension of the single fracture. The five shadings used in the figure illustrate the varying aperture values in five steps from $b < 22$ μm to $b > 116$ μm.

Now let us apply a pressure difference across the single fracture saturated with water. In Figure 3a let the pressure on the left side be P_1; on the right side P_2, and the top and bottom sides be closed to water flow. If we assume that locally the permeability to fluid flow is proportional to the square of the local apertures, then the resistance to flow between two adjacent mesh elements i and j (Figure 3b) is $R_{ij} = 6\mu \frac{\Delta x}{\Delta y}\left[\frac{1}{b_i^3} + \frac{1}{b_j^3}\right]$, where μ is value of fluid viscosity. Then the fluid flow through the fracture can be calculated by solving a matrix equation relating the pressures at all the points in the fracture. A similar calculation can also be made if we apply P_1 and P_2 to the top and bottom sides of the fracture with the left and right sides closed to water flow.

Figure 4a shows the flow when the pressure difference is applied on the left and right sides of the fracture and Figure 4b shows the flow when the pressure difference is applied on the top and bottom sides of the fracture. For illustrative purposes we have shown the flow pattern by arbitrarily making the thickness of the lines in the figure to be proportional to the square root of the local flow rates. The flow rates at different locations in the fracture vary greatly, by orders of magnitude. The exit flow rates range from 0.001 to 100 units and are shown in Figures 5a and 5b. It is apparent that in both the left-right and top-bottom flow patterns preferred flow paths are present, though they are different geometrically for the two flow directions. These preferred flow paths are what we called channels, along which the apertures are variable. Thus, these channels are NOT physical large-flow tubes embedded in the fracture plane, but are preferred flow paths, in the sense of stream-lines or stream-tubes in the hydraulic potential theory, due to the strong variation of the aperture and hence, permeability value.

The channeling effects described here occur in addition to the physical or structural large-permeability channels in the fractured medium, such as those observed near the intersection of orthogonal fractures (Abelin et al., this volume 1988).

Now, as can be seen in Figures 4a and 4b, for the same fracture, flow channels observed for applied left-right and top-bottom pressure differences are quite different geometrically. What, then, characterizes these channels? To study this, we calculate tracer transport through the fracture using the particle tracking method (see e.g. Smith and Schwartz, 1980 and Moreno et al. 1988). A sufficiently large number of particles, in our case ten thousand, are introduced on the high pressure side of the fracture and are allowed to travel through the system with the probability of entering a particular flow section in the fracture proportional to the local flow rate. Also, when a particle comes to an intersection with two or three outgoing flow sections, a Monte Carlo method is used to assign the particle to one of the flow directions with probabilities weighted by their respective flow rates. As each of the particles travels through the fracture, the apertures it goes through are recorded. These build up the statistics of the aperture values of the channels. The results are shown as aperture density distribution functions in Figure 6. The dashed line gives the probability density distribution of apertures over the entire 2D plane of the fracture. The two solid lines give the aperture density distribution seen by the particles in the left-right and top-bottom flow directions respectively.

The tracer particles tend to travel through large apertures and avoid small apertures of the 2D fracture aperture distribution. However, they cannot avoid the small apertures altogether and thus there is some finite probability of flow through apertures one or two orders of magnitudes smaller than the large apertures most particles travel through. Now, the aperture density distribution functions for left-right and for top-bottom tracer transport are found to be very similar. This is not obvious a priori, because the channels in the two cases represent quite different flow paths (Figures 4a and 4b). Thus we arrive at the interesting result that channels of tracer transport in the fracture system are characterized by the same aperture density distribution. We shall show how this information can be used in a later section.

The conclusion of the above study is that to understand tracer transport in such a highly heterogeneous system, we can consider transport channels which are

characterized by an aperture probability distribution function, rather than specific (deterministic) flow paths.

Tracer breakthrough curves and the case for line (areal) or multi-point measurements

Using the particle tracking method, we can also calculate the tracer breakthrough curves. The time each particle takes to arrive at the low-pressure side of the single fracture is calculated by adding up the time it takes to traverse each step in the fracture (Moreno et al. 1988). The composite of the arrival times for all the particles forms the tracer breakthrough curves shown in Figure 7, which shows the percentage of particle arrivals versus time normalized by the mean arrival time of all the particles. In a tracer test, the vertical axis would be proportional to exit concentration. In this figure, seven curves are shown, representing four realizations of 2D fractures for $\lambda/L = 0.1$ and three for $\lambda/L = 0.4$. Thus this figure displays the sensitivity of the tracer breakthrough curves to two values of spatial correlation length, λ, and the different realizations that are statistically generated from the same input parameters, $\bar{b}$ and σ.

Figure 7 presents the dispersion of tracer particles through the fracture due to the large aperture variations. This dispersion acts in addition to the molecular diffusion and Taylor dispersion, which are set equal to zero in our calculation, and also in addition to dispersion due to matrix diffusion, surface sorption/desorption and other processes. The dispersion shown in this figure has two sources, one major and one minor. The minor source is tortuosity, which is the fact that the tracer particles travel by paths of different lengths. In our case, as in usual porous medium flow, the tortuosity effect results in path lengths that differ from the average by a factor approximately between 1 and 2. The major source causing the dispersion in these results is the strongly varying flow rates in the flow channels, due to aperture constrictions along the particle flow paths. Such aperture constrictions cause flow rates to differ by orders of magnitude from each other.

It is of interest to note that all seven curves in Figure 7 fall within a small band. This shows that the results are not sensitive to the two values of λ/L and to the different realizations used. We believe that this is due to the fact that we have considered tracer input and output along a line with a length equal to several spatial correlation lengths, thus averaging over strong local concentration variations of tracer emergence. Such large variations are to be expected based on the channeling character of tracer transport through the fracture system.

To illustrate the discussion we performed calculations for a number of realizations in which the same fluid flow field over the 2D fracture is used, but tracer particles are released only within a section length $s < L$ at a few high-flow locations along the high pressure side and collected at a few high-flow positions on the low pressure side. See Figure 8, for example. The collection length is assumed to be also s. Calculations were made for $s/L = 0.1$, 0.33 and 0.5. Figure 9 shows tracer breakthrough curves for $s/L = 0.1$ for one of the realizations with $\lambda/L = 0.1$. Here tracers are released at two alternative locations, A and B, and collected at three alternative locations, D, E and F (Figure 8). These locations are chosen because of their relatively large local flow rates. At each exit section, concentration, C, was calculated by dividing the accumulative exit particle number by the local flow rate. The maximum input concentration, C_o, is defined as the total number of tracer particles used in the calculation divided by the flow rate in the input section. The plot in Figure 9 is C/C_o versus time of arrival, t, at the exit sections. Note that C/C_o does not reach a value of 1 because of mixing of water from the tracer-injection section with the remainder of water inflow from high pressure side.

Several comments on the calculations need to be made. First, the exit flow rates at the three exit sections are quite different. They are given by Q = 26, 53, 37 units, respectively. Second, the initial arrival times of the six possible tracer paths do not correlate with the linear distances between the tracer-injection section and the collection section. For example, the earliest arrival time corresponds to the case with linear transport distance of 1.04 L (tracer from B to E), and this is about half of the arrival

time for a case with a slightly shorter linear transport distance of 1.005 L (tracer from B to F). Such non-correlation between initial arrival times and linear transport distances has often been observed in the field. A recent example may be found in the data from the Fanay-Augères field tracer experiment (Cacas et al., this volume, 1988).

One may define a measure for the dispersion displayed in Figure 9 as given by $(t_{0.9} - t_{0.1}) / t_{0.5}$, where t_x is the time of arrival when the concentration reaches a fraction x of the maximum concentration value at large times. This empirical definition of dispersion has the advantage that it is independent of a model for the system. For the particular case of the porous medium model, this definition has been shown to relate to the dispersivity through the Peclet number (Neretnieks, 1983). Let us take the cases shown in Figure 9, and calculate the value of the dispersion measure as defined above for each case. The results obtained are spread out over a factor of 3 from each other (see Figure 10 for s = 0.1 L). However, if we carry out the same exercise with the tracer collection section length increased from s/L = 0.1 to 0.33 and to 0.50, the spread of the dispersion measure is greatly reduced. This is shown in Figure 10. Recall that in this case the spatial correlation length is $\lambda/L = 0.1$.

The results in Figure 10 suggest that line measurements with line section lengths corresponding to a few correlation lengths may yield more stable values for the dispersion measure, which may then be studied for its dependence on the basic parameters $\bar{b}$ and σ.

Interpretation of 2D transport in terms of a Channel Model

In an earlier section we showed that the transport of tracer particles through a 2D fracture of strongly varying apertures takes place in variable-aperture channels (in the sense of stream-tubes in the potential theory), which are characterized by an aperture probability distribution function with parameters $\bar{b}$ and σ.

In this section we shall demonstrate how a group of one-dimensional channels with apertures obeying the aperture probability distribution function can reproduce the detailed two-dimensional results. In Figure 6, we show that the apertures seen by tracer particles as they travel under a pressure difference through the 2D fracture obey an aperture distribution function shown by the solid line. Let us start with this aperture distribution function and construct 1D variable-aperture channels statistically (Tsang and Tsang, 1987; Tsang et al. 1988). A system of 40 1D channels were generated and they are interpreted as 40 possible flow paths taken by the tracer particles traveling through the 2D fracture. The choice of 40 as the number of 1D channels is somewhat arbitrary, though it should be large enough to produce a smooth tracer breakthrough curve on the exit side of the fracture. A pressure difference is applied across these 1D channels, each of which will carry a different flow rate with a different travel time for the tracer particles. The tracer breakthrough curve is obtained by accounting for arriving particles from this system of 1D channels. 40 realizations of this system of 40 1D channels were generated and for each, the tracer breakthrough curve was calculated. The results are shown in Figure 11, where the mean of the 40 breakthrough curves for the 40 realizations is shown as the long-dash broken curve, with the limit of the spread of the 40 curves indicated by a horizontal bar. The solid curve in the figure is the result of the detailed 2D tracer transport calculations (Figure 7) with the horizontal bar indicating the limit of the spread of calculated values for eight realizations.

We also took the same initial aperture density distribution and constructed a system of constant-aperture channels and computed the breakthrough curves. These are channels, each of which have a constant aperture, but with values different from each other. (This can be interpreted as the so-called perfectly stratified reservoir model). The results are shown as the short-dashed broken curve in Figure 11. Finally, if the entire fracture is a parallel plate with only one constant aperture, then the result would be a step with concentration 0 for $t/t_m < 1$ and 100% for $t/t_m \geq 1$, implying a piston flow with zero dispersion. The results for the tracer breakthrough through such a

parallel plate representation of a single fracture are shown as the dot and dash curve in the figure. The better fit of the 1D Channel Model to the detailed 2D results is apparent in this figure.

Figure 11 is plotted with time on the horizontal axis normalized to the mean residence time t_m in order to compare the dispersion predicted from the different models. The actual values of mean residence time from the different models are presented in Table 1. The second column gives the expected values obtained by dividing total fracture volumes by the calculated total flow rates in two dimensions. The third column gives the mean particle residence times from the breakthrough curves derived from particle tracking in two dimensions. These agree within a few percent of the values in column 2. The fourth column gives the mean residence times from the breakthrough curves derived from the one-dimensional variable-aperture channel model. We note that the mean residence times are within a factor of two as those derived from the actual two-dimensional transport. The last column gives the mean residence times obtained from the breakthrough curves derived from a system of constant aperture channels. The mean residence times in this last column are typically two to three orders of magnitude smaller than those predicted from both the two-dimensional and one-dimensional variable-aperture channel calculations. This is easy to understand since in the constant-aperture channel representation, the larger the aperture, the shorter the residence time, therefore the average is heavily weighted by the residence times of the largest constant aperture channels.

The qualitative agreement between the results from one-dimensional variable-aperture channel model and the two-dimensional calculations shown in both Figure 11 and Table 1 is good. This implies that as far as tracer transport is concerned, breakthrough curves for a 2D fracture with variable apertures can be obtained by a model of 1D variable-aperture channels, which are characterized by an aperture probability distribution function, with just two parameters, b and σ.

Summary and Conclusions

Tracer transport through fractured rocks should no longer be envisioned as transport through a system of interconnecting parallel-plate fractures. The strongly varying apertures of these fractures result in preferred paths of fluid and tracer flow in the fractures. These have been observed in field and laboratory experiments, and are referred to as channels. Thus channels defined this way are not rigidly set pathways for tracer transport, but are the preferred flow paths in the sense of stream-tubes in the potential theory. These channels are present in addition to physical or structural channels along lines of high permeability, such as those occurring at the fracture intersections.

It is shown in this paper that such variable-aperture channels can be characterized by an aperture probability distribution function with parameters $\bar{b}$ and σ, and not by the exact deterministic geometric locations. We demonstrated that the 2D tracer transport in a fracture can be calculated by a model of a system of 1D channels characterized by this distribution function only. In general, transport through multiple fractures may also be calculated by a model of a system of 1D channels characterized by an aperture distribution function, which is built up of apertures from all the fractures.

Due to the channeling character of tracer transport in fractured rock, random point measurements of tracer breakthrough curves may give results with a wide spread in value due to statistical fluctuations. The present paper suggests that such wide spread can probably be greatly reduced by making line/areal (or multiple) measurements covering a few spatial correlation lengths. We believe much work remains to be done along this line both by theoretical studies and by numerical experiments.

Acknowledgements

Collaboration and discussions with L. Moreno and I. Neretnieks of The Royal Institute of Technology, Stockholm, Sweden are much appreciated. The review and

comments from C. Carnahan, C. Doughty and J. Noorishad of Lawrence Berkeley Laboratory are gratefully acknowledged. The work is supported in part by the Assistant Secretary for Energy Research, Office of Basic Energy Sciences, Division of Engineering and Geosciences, and by the Office of Civilian Radioactive Waste Management, Office of Geologic Repositories, Engineering and Geotechnology Division, through the U.S. Department of Energy Contract DE-AC03-76SF00093.

Selected References

Abelin, H., Bergersson, Gidlund, J., Moreno, L., Neretnieks, I., Widen, H., and Andersson, J., 1988, Results of some large scale in situ tracer experiments in a drift at the Stripa Mine, Proceedings of International Conference on Fluid Flow in Fractured Rocks, Atlanta, Georgia, May 16-18, pp.

Abelin, H., Gidlund, J. and Neretnieks, I., 1982, Migration in a single fissure. *Scientific Basis for Nuclear Waste Management* V, p. 529. North Holland Elsevier Science Publishers, New York.

Bourke, P. J., 1987, Channeling of flow through fractures in rock, Proceedings of GEOVAL-87, International Symposium, Stockholm, Sweden, April 7-9.

Cacas, M. C., Ledoux, E., and de Marsily G., 1988, Calibration and validation of a three-dimensional stochastic network model on a large scale experiment with flow measurements and tracer tests performed in the uranium mine of Fanay-Augeres, Proceedings of International Conference on Fluid Flow in Fractured Rocks, Atlanta, Georgia, May 16-18, pp.

Gale, J. E., 1988, Characterizing the geometry of fracture systems for flow and transport studies in fractured rock masses, Proceedings of International Conference on Fluid Flow in Fractured Rocks, Atlanta, Georgia, May 15-18, pp.

Gentier, S., 1986, Morphologie et comportement hydromecanique d'une fracture naturelle dans un granite sous contrainte normale, Doctoral Thesis, U. d'Orleans, France.

Moreno, L., Tsang, Y. W., Tsang, C. F., Hale, F. V., and Neretnieks, 1988, I., Flow and tracer transport in a single fracture: A stochastic model and its relation to some field observations, LBL-25049, accepted for publication in *Water Resources Research.*

Neretnieks, I., 1983, A note on fracture flow dispersion mechanisms in the ground, *Water Resources Research,* 19 (2), pp. 364-370.

Neretnieks, I., 1985, Transport in fractured rocks, Proceedings, Memoires of the 17th International Congress of International Association of Hydrologists, Vol. XVII, 301-318, International Association of Hydrologists, Tucson, Arizona.

Smith, L. and Schwartz, F. W., 1980, Mass transport, 1: A stochastic analysis of macroscopic dispersion, *Water Resources Research,* 16 (2), pp. 303-313.

Tsang, Y.W., 1984, The effect of tortuosity of fluid flow through a single fracture, *Water Resources Research,* 20 (9), pp. 1209-1215.

Tsang, Y. W., and Tsang, C. F., 1987, Channel model of flow through fractured media, *Water Resources Research,* 23 (3), pp. 467-479.

Tsang, Y. W., Tsang, C. F., Neretnieks, I., and Moreno, L., 1988, Flow and tracer transport in fractured media — A variable-aperture channel model and its properties, LBL-25048, accepted for publication in *Water Resources Research.*

Table 1 Mean residence times for a number of runs or realizations, calculated from (a) 2D fracture volume divided by total calculated flow rate, (b) mean particle travel time from 2D calculation, (c) mean travel time from a system of 1D variable-aperture channels, and (d) mean travel time from a system of constant-aperture channels.

Run	Mean Residence Time (arbitrary units)			
	Fracture Volume / 2-D Flow Rate	2-D Particle Tracking	Variable-Aperture 1-D Channels	Constant-Aperture 1-D Channels
511	0.59	0.59	0.82	0.004
512	1.46	1.49	1.64	0.012
513	0.35	0.34	0.39	0.007
514	0.33	0.33	0.41	0.006
541	0.07	0.07	0.06	0.0005
542	2.29	2.30	3.10	0.007
543	0.86	0.85	1.15	0.0047
544	0.30	0.30	0.35	0.003

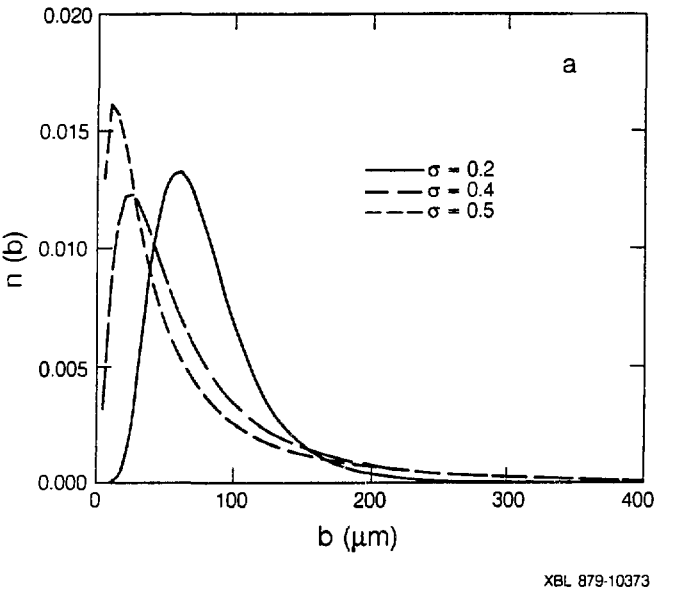

Figure 1 Lognormal distributions with $\bar{b} = 80$ μm and $\sigma = 0.2$, 0.4 and 0.5, plotted on a linear scale.

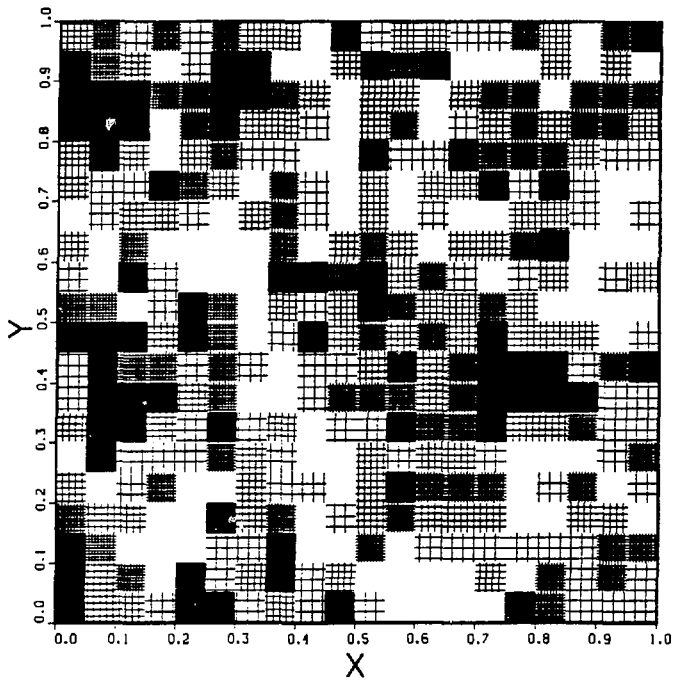

XBL 887-10344

Figure 2 Statistically generated apertures with a spatial correlation length λ of 0.1L in the plane of a single fracture of linear dimension L. The shadings are given in five levels from small apertures (dark) to large ones (white). The dividing values correspond to the logarithm of apertures given by 1.33, 1.59, 1.81, 2.07, with apertures in μm.

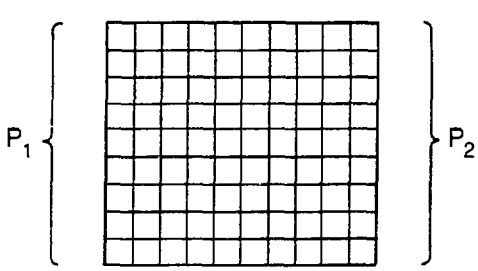

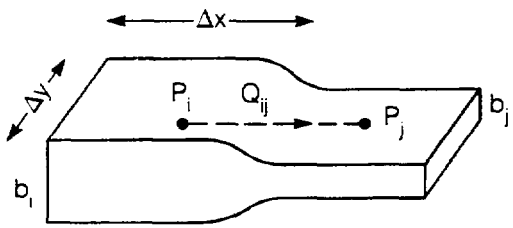

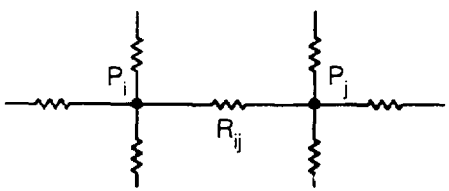

$$R_{ij} = 6\mu \frac{\Delta x}{\Delta y} \left(\frac{1}{b_i^3} + \frac{1}{b_j^3} \right)$$

XBL 873-10019

Figure 3 (a) Schematic diagram for flow through a single fracture with different aperture values assigned areas bounded by grid lines.
(b) Schematic diagram for two adjacent elements of different apertures, b_i and b_j and the fluid flow Q_{ij}, between them.
(c) Resistance to fluid, R_{ij}, in an electric analog, in terms of apertures, dimensions of the elements and fluid viscosity μ.

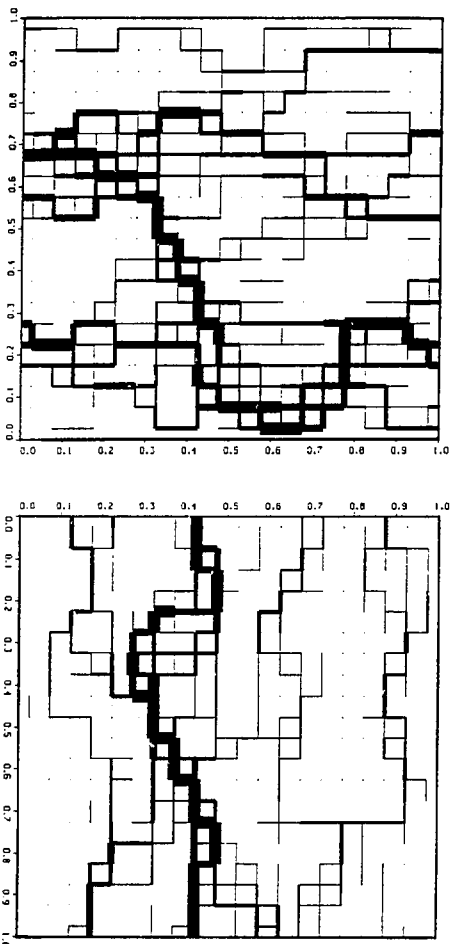

Figure 4 (a) Fluid flow rates for the fracture with aperture variations as shown in figure 2. The thickness of the lines is proportional to the square root of the flowrates. Pressure difference is applied from left to right. (b) Same as (a), but with pressure difference applied from top to bottom.

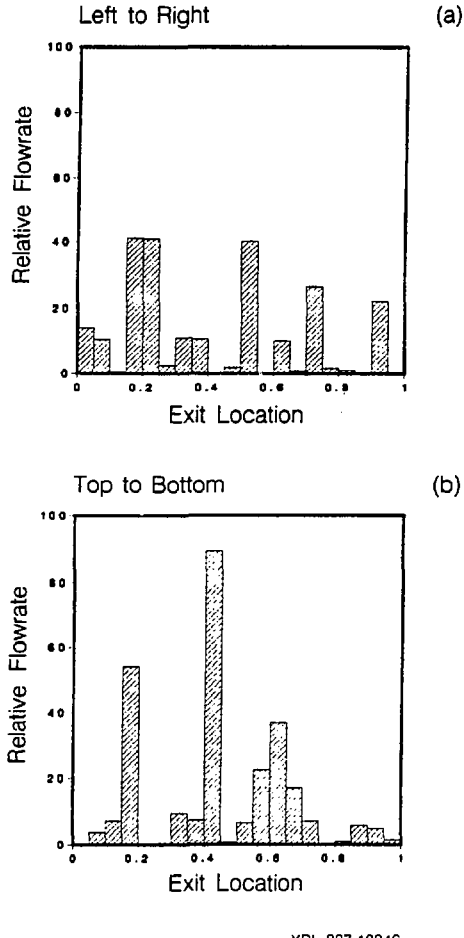

Figure 5 Histograms of flow rates along the exit line corresponding to Figures 4a and 4b respectively.

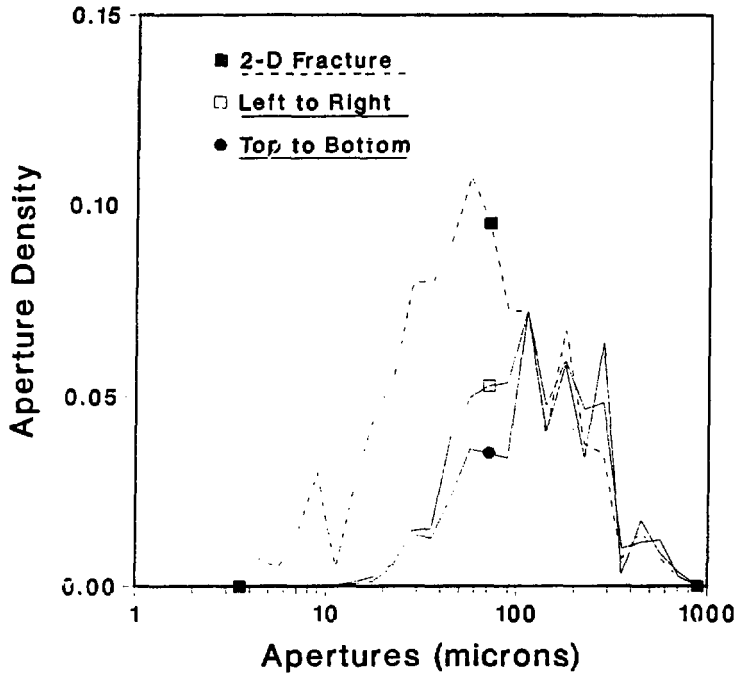

Figure 6 The aperture probability density distribution for (a) apertures over the entire 2D fracture plane corresponding to Figure 2; (b) apertures along particle flowpaths with left-right pressure difference; and (c) apertures along particle flowpaths with top-bottom pressure difference.

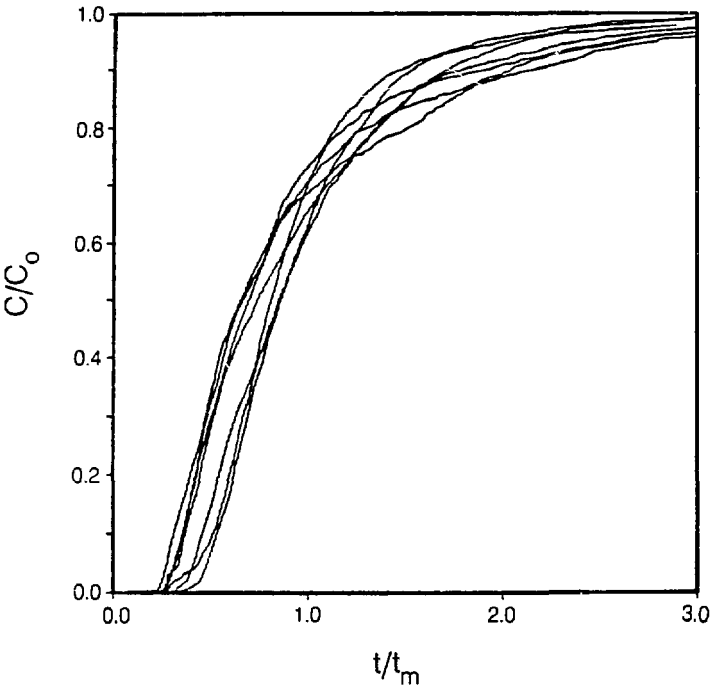

Figure 7 Tracer breakthrough curves from particle tracking with time normalized to the mean residence time, t_m, of all the particles. Seven realizations of the generated fracture aperture distributions are used, including the case shown in Figure 2. Among the seven, four has $\lambda = 0.1L$ and three has $\lambda = 0.4L$. All curves fall within a narrow band of each other.

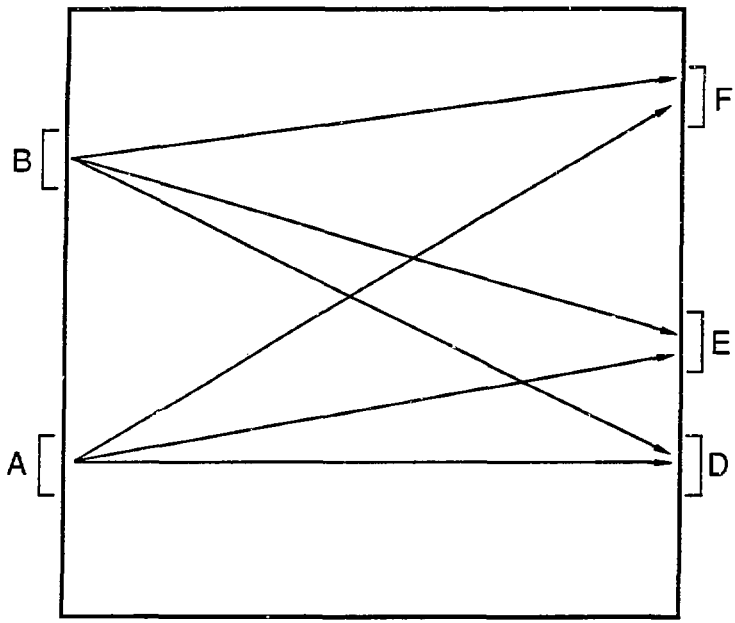

XBL 887-10330

Figure 8 Schematic diagram illustrating "point" measurements of tracer transport. Based on one of the realizations of a fracture with variable apertures with an applied left-right pressure difference, tracers are deposited at A and B and collected at D, E, and F. Points A, B, D, E and F are chosen at locations of large entrance or exit flow rates and each is associated with a section length of 0.1L.

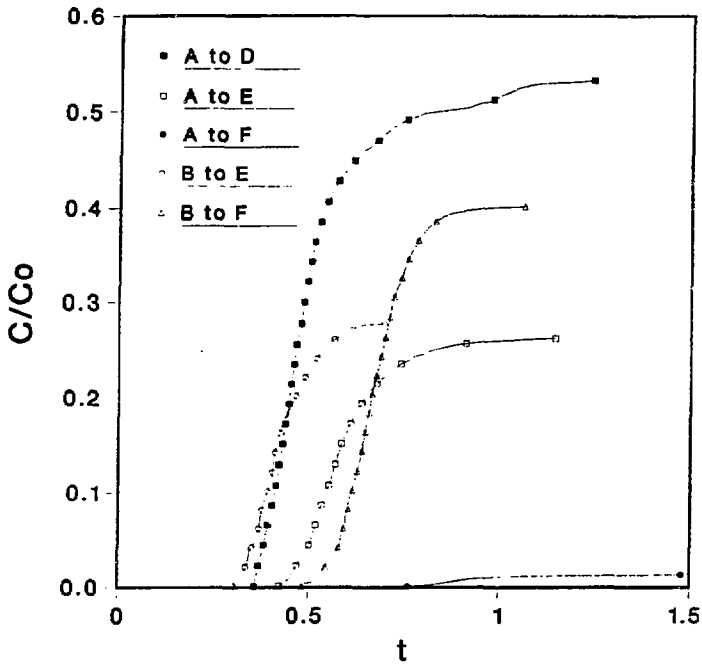

Figure 9 Tracer breakthrough curves for cases shown in Figure 8, with the section length for tracer entrance or exit equal to 0.1L.

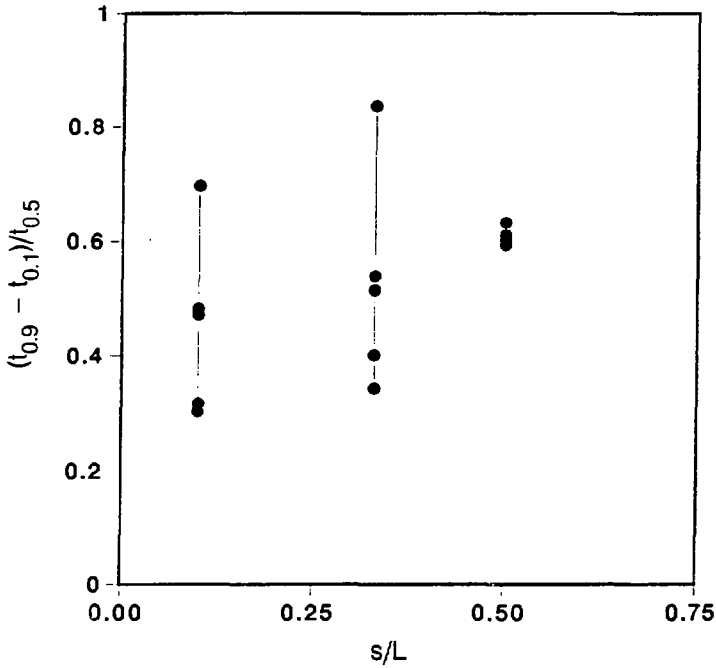

XBL 887-10350

Figure 10 The tracer dispersion measure, $(t_{0.9} - t_{0.1}) / t_{0.5}$, as a function of the section length for tracer entrance or exit.

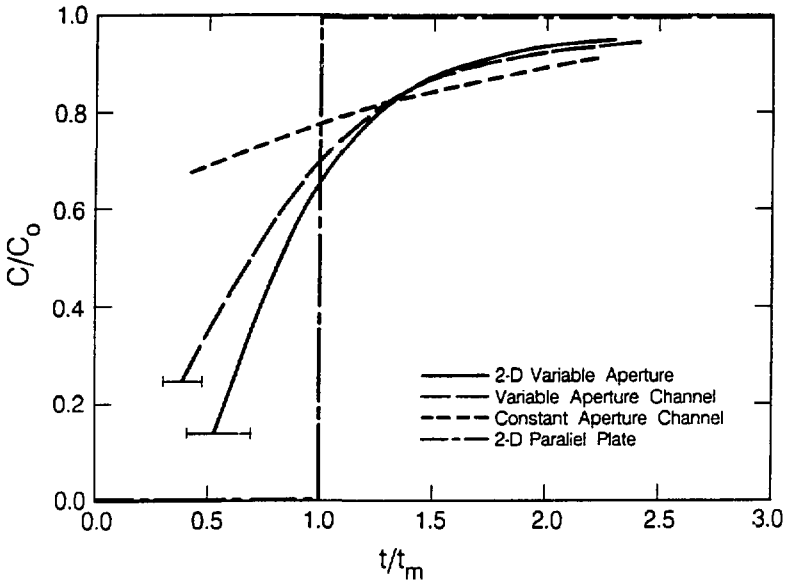

Figure 11 Tracer breakthrough curves from (a) 2D calculation, (b) 1D variable-aperture channel calculation, (c) constant-aperture channel calculation, and (d) parallel-plate fracture calculation. Horizontal bars give the limits of values from seven realizations each for cases (a) and (b).